

Brownian ratchet in a thermal bath driven by Coulomb friction

Andrea Gnoli

*Istituto dei Sistemi Complessi - CNR, via del Fosso del Cavaliere 100, 00133 Rome, Italy and
Istituto dei Sistemi Complessi - CNR and Dipartimento di Fisica,
Università "Sapienza", p.le A. Moro 2, 00185 Rome, Italy*

Alberto Petri, Fergal Dalton, and Giorgio Pontuale

Istituto dei Sistemi Complessi - CNR, via del Fosso del Cavaliere 100, 00133 Rome, Italy

Giacomo Gradenigo, Alessandro Sarracino, and Andrea Puglisi

*Istituto dei Sistemi Complessi - CNR and Dipartimento di Fisica,
Università "Sapienza", p.le A. Moro 2, 00185 Rome, Italy*

The rectification of unbiased fluctuations, also known as the ratchet effect, is normally obtained under statistical non-equilibrium conditions. Here we propose a new ratchet mechanism where a thermal bath solicits the random rotation of an asymmetric wheel, which is also subject to Coulomb friction due to solid-on-solid contacts. Numerical simulations and analytical calculations demonstrate a net drift induced by friction. If the thermal bath is replaced by a granular gas, the well known granular ratchet effect also intervenes, becoming dominant at high collision rates. For our chosen wheel shape the granular effect acts in the opposite direction with respect to the friction-induced torque, resulting in the inversion of the ratchet direction as the collision rate increases. We have realized a new granular ratchet experiment where both these ratchet effects are observed, as well as the predicted inversion at their crossover. Our discovery paves the way to the realization of micro and sub-micrometer Brownian motors in an equilibrium fluid, based purely upon nano-friction.

PACS numbers: 02.50.Ey, 05.20.Dd, 81.05.Rm

From microscopic organisms to muscle fibres, from electric motors to power stations, the biosphere, our society and our lives critically depend on the conversion of energy to mechanical work. Thermodynamics provides precise and well established rules for energy conversion in macroscopic systems but these rules become blurred at small scales when thermal fluctuations play a decisive role [1]. Extracting work under such conditions requires subtle strategies radically different from those effective in the macroscopic world [2–7]. Within this framework, the theory of Brownian motors deals with the rectification of thermal fluctuations, a goal which can only be achieved in the presence of dissipation [8–13]. An interesting class of systems, where both dissipation and fluctuations are relevant, is represented by granular media [14, 15]. Indeed, interactions in a granular system are inherently dissipative, and because of its small number of constituents when compared with molecular gases or liquids, a granular fluid presents large fluctuations. The additional break of spatial symmetry is sufficient for a motor effect to be generated as demonstrated in a series of experiments [16–18] and theoretical works [19–24].

In previous work the main source of dissipation was provided by the inelasticity of collisions, a property normally not present at micro or nanometric scales. The remarkable result of our study is a new minimal model for a motor where energy is extracted from an equilibrium bath and dissipated only through Coulomb friction [25]. Friction is therefore demonstrated to be an unexpectedly efficient source of dissipation, that is able to rectify

unbiased fluctuations also in the case of *fully elastic* collisions. Such a model can therefore be exploited in micro and nano apparatuses where friction is still present [26].

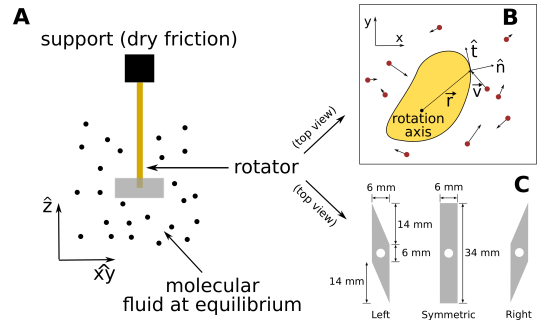


FIG. 1: A) Sketch of the model, front view. B) Top view, with explanation of quantities used in the text for a generic-shaped rotator. C) Top view, with specific shapes used in the simulations and in the experiment.

Our model, described pictorially in Fig. 1a, consists of: a wheel of mass M and inertia I , rotating with angular velocity ω around a fixed axis (say \hat{z}). The wheel is immersed in an equilibrium fluid and collides with the molecules of mass m , and is subject to a viscous drag $-\Gamma_{visc}\omega$ and, most importantly, to a Coulomb friction torque $-F_{friction}\sigma(\omega)$ (where $\sigma(x)$ is the sign function), due to solid-on-solid contacts within its support, e.g. a spherical bearing. The equation of motion for the angular

velocity $\omega(t)$ of the wheel, therefore, reads

$$\dot{\omega}(t) = -\gamma_a \omega(t) - \sigma[\omega(t)]\Delta + \eta_{coll}(t) \quad (1)$$

where $\gamma_a = \Gamma_{visc}/I$, $\Delta = F_{friction}/I$ and $\eta_{coll}(t)$ is the random force due to collisions with the molecules of the bath. The wheel is a cylinder parallel to the rotation axis \hat{z} . Its base in the plane $\hat{x}\hat{y}$ (shown in Fig. 1b for a generic shape) can be symmetric or asymmetric for inversion of one of the two axis (\hat{x} or \hat{y}). The two specific shapes taken in consideration here, one symmetric and other asymmetric, are drawn in Fig. 1c. The velocities of the molecules are distributed according to the Maxwell-Boltzmann distribution, with the only parameter being the “thermal” velocity $v_0 = \sqrt{\langle v^2 \rangle}$, where v is a component of the velocity vector on the $\hat{x}\hat{y}$ plane. The molecular bath is also characterized by its number density n . The main parameter for the collision between the wheel and the molecules is the total cross section Σ . The collision rule, given in details in the Supplemental Material [27], conserves total angular momentum and may dissipate part of the total kinetic energy, according to the value of the restitution coefficient $\alpha \in [0, 1]$. We will show that our model exhibits the ratchet effect even in the case of fully elastic collisions ($\alpha = 1$), and even if the viscous force is removed ($\gamma_a = 0$). The choice of a more general (possibly inelastic) collision rule and the presence of a weak viscous damping is necessary to account for the results of the granular experiment described below. For consistency with the experiment, the viscous force (if present) is assumed to be small enough that $\gamma_a|\omega| \ll \Delta$ for most of the values of ω .

When the range of interactions with the molecules is short enough (as in the hard-core case), only two time-scales are relevant in the system: 1) the mean stopping time due to environmental dissipation, dominated by Coulomb friction, $\tau_\Delta = \frac{\langle |\omega| \rangle_{pc}}{\Delta} \sim \frac{\epsilon v_0}{R_I \Delta}$, where $\langle \cdot \rangle_{pc}$ denotes a post-collisional average, $R_I = \sqrt{I/M}$ is the radius of inertia and $\epsilon = \sqrt{m/M}$; 2) the mean free time between two collisions $\tau_c \sim \frac{1}{n\Sigma v_0}$. We therefore use as main control parameter

$$\beta^{-1} = \frac{\epsilon n \Sigma v_0^2}{\sqrt{2\pi} R_I \Delta} \approx \frac{\tau_\Delta}{\tau_c} \quad (2)$$

which is an estimate of the ratio of those two time-scales, as verified by simulations [27]. As already noticed [22, 23], when $\beta^{-1} \gg 1$ ($\tau_c \ll \tau_\Delta$) the dynamics of the rotator is dominated by collisions and friction is negligible (frequent collisions limit, denoted in the following by FCL); in the opposite limit $\beta^{-1} \ll 1$ ($\tau_c \gg \tau_\Delta$, rare collisions limit, RCL) the rotator remains most of the time at rest and is rarely perturbed by collisions acting as independent random excitations.

The complex behaviour of the model is simplified in the diluted limit, when Molecular Chaos can be assumed. With such an assumption, the probability density function (pdf) $p(\omega, t)$ for the angular velocity is

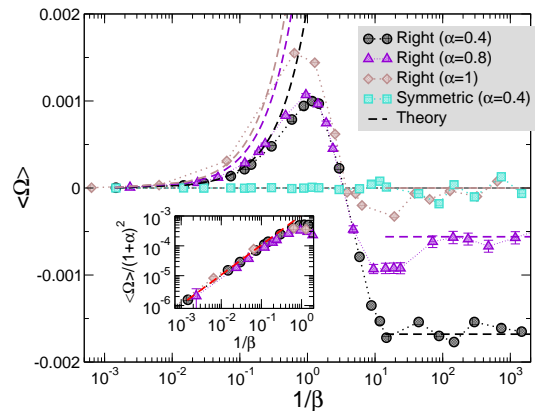


FIG. 2: Simulations under the assumption of Molecular Chaos. The rescaled average angular velocity $\langle \Omega \rangle$ is shown as a function of β^{-1} . Theoretical expectations in the FCL and RCL are marked by dashed lines. The lower inset zooms in the RCL region. Simulations are performed using shapes and dimensions of Fig. 1c, $\Delta = 10$, $\gamma_a = 0$, $R_I/\epsilon = 10^3$ and $v_0 = 100$ in arbitrary units (varying $n\Sigma$ to obtain a variation of β^{-1}).

fully described by the following linear Boltzmann equation [22, 24, 28]

$$\partial_t p(\omega, t) = \partial_\omega [(\Delta \sigma(\omega) + \gamma_a \omega) p(\omega, t)] + J[p, \phi] \quad (3a)$$

$$J[p, \phi] = \int d\omega' W(\omega|\omega') p(\omega', t) - p(\omega, t) f_c(\omega), \quad (3b)$$

where we introduce the rate $W(\omega'|\omega)$ for the transition $\omega \rightarrow \omega'$ and the velocity-dependent collision frequency $f_c(\omega) = \int d\omega' W(\omega'|\omega)$. The rate $W(\omega'|\omega)$, given explicitly for hard-core interactions in [27], depends on the velocity distribution of the gas particles, on the restitution coefficient α , on the rotator cross section and on the density of the gas.

A first insight into Eq. (3) is obtained by Direct Simulation Monte Carlo [27, 29], whose results are summarized in Fig. 2, always keeping $\gamma_a = 0$. The Figure shows the average velocity of the ratchet rescaled by the ideal “thermal” velocity, i.e. $\langle \Omega \rangle = \frac{R_I}{\epsilon v_0} \langle \omega \rangle$, for several values of α and different shapes. Our main, unprecedented, result is the existence of an average drift, i.e. a motor effect, in the case of elastic collisions, provided that the shape is asymmetric (curve with diamond symbols). This effect is independent of the presence of the viscous damping, which very weakly affects the results of the simulation. In the elastic case, the average drift disappears for large β^{-1} , where the effect of friction is washed out by highly frequent collisions and the system equilibrates with the bath. Remarkably, the ratchet effect starting from the RCL increases, in absolute value, when β^{-1} increases, so that it must go through a maximum. We interpret such a maximum as a kind of *stochastic resonance*: the rotator switches from the “drift” state to the “rest” state on the time-scale τ_Δ and switches back to the “drift” state on

the time-scale τ_c . When the two scales synchronize with each other, the total time spent in the “drift” state is maximized, as well as its average velocity.

As demonstrated in previous studies [19, 20], in the inelastic case ($\alpha < 1$) a ratchet effect survives also in the FCL: interestingly, it takes different signs with respect to the RCL. Therefore, the crossover between these two limits requires the presence of an inversion point.

It is possible to have an analytical account of the two opposite RCL and FCL limits [22, 24]. When the mass of the rotator is large, $\epsilon \ll 1$ the FCL is perturbatively reduced to a Brownian approximation and the average drift has already been computed [24] giving

$$\langle \Omega \rangle = \epsilon \sqrt{\frac{\pi}{2}} \frac{1 - \alpha}{4} \mathcal{A}_{FCL} \quad (4a)$$

$$\mathcal{A}_{FCL} = -\frac{\langle g^3 \rangle_{surf}}{\langle g^2 \rangle_{surf}}, \quad (4b)$$

where the asymmetry of the rotator is represented by \mathcal{A}_{FCL} which is 0 for a symmetric rotator; above we have used the shorthand notation for the uniform average along the perimeter (denoted as “surface”) of the base of the wheel $\langle \cdot \rangle_{surf} = \int_{surf} \frac{ds}{S}$ (S being the total perimeter [27]), while $g = \frac{v \cdot \hat{t}}{R_I}$; see Fig. 1b for an explanation of symbols. This formula predicts zero net drift either with elastic collisions ($\alpha = 1$) or with a symmetric rotator ($\mathcal{A}_{FCL} = 0$), as expected from symmetry arguments. Most importantly, it predicts a constant value, as verified in the numerical simulations. This implies $|\langle \omega \rangle| \sim v_0$ for the *dimensional* angular velocity.

The study of the RCL leads to remarkably different predictions. In such a limit, the dynamics after each collision event produces an increment of the angular position of the rotator $\Delta\theta$ which depends on the velocity \mathbf{v} of the gas particle, precisely on its projection $v = \mathbf{v} \cdot \hat{n}$, and on the point of impact represented by its curvilinear abscissa s . The formula is $\Delta\theta(v, s) = \sigma(\omega_0) \frac{\omega_0^2}{2\Delta}$ with $\omega_0 = -(1 + \alpha) \frac{v}{R_I} \frac{\epsilon^2 g}{1 + \epsilon^2 g^2}$. Following the calculations detailed in [27], one obtains the formula for the rescaled average velocity of the ratchet

$$\langle \Omega \rangle = \sqrt{\pi} (1 + \alpha)^2 \beta^{-1} \epsilon^2 \mathcal{A}_{RCL} \quad (5a)$$

$$\mathcal{A}_{RCL} = \left\langle \frac{\sigma(g) g^2}{(1 + \epsilon^2 g^2)^2} \right\rangle_{surf}, \quad (5b)$$

where $\mathcal{A}_{RCL} = 0$ for symmetric shapes of the rotator. Eq. (5) shows that a non-zero drift is achieved *for any value of the restitution coefficient*: even in the (ideal) elastic case, Coulomb friction alone produces the desired ratchet effect provided that the shape of the rotator is not symmetric, i.e. that $\mathcal{A}_{RCL} \neq 0$. Note that the limit of vanishing dry friction ($\Delta \rightarrow 0$) is singular in formula (5a), since in the absence of dissipation between collisions the stopping time becomes infinite, $\tau_\Delta \rightarrow \infty$, and the as-

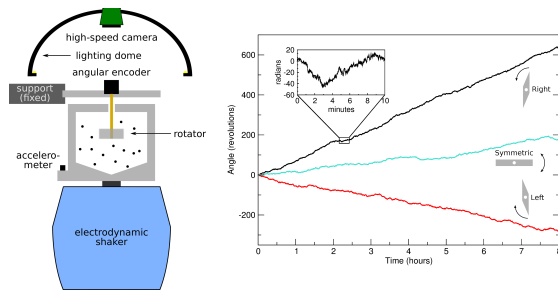


FIG. 3: Real experiment. A) Experimental setup. B) The angular position of the rotator as a function of time, highlighting the ratchet effect for the asymmetric rotator. The inset shows an enlargement (ten minutes) extracted from an asymmetric (right) experiment. For these experiments the value of maximum acceleration, normalized by gravity, is 13.

sumption of “rare collisions” breaks down. Equally interesting, the shape factor \mathcal{A}_{RCL} , determining the intensity and drift direction in the RCL, can take *opposite sign* with respect to the shape factor \mathcal{A}_{FCL} in the FCL formula. This is precisely the case for our chosen shape, see Fig. 1c. Moreover, the magnitude of the drift is predicted to increase with β^{-1} as seen in the numerical simulations for small β^{-1} . This corresponds to $|\langle \omega \rangle| \sim v_0^3$. Both the predictions for the RCL and for the FCL are superimposed on the results (elastic and inelastic) of the numerical simulations in Fig. 2, demonstrating excellent agreement in their respective limits. We remark that if friction is removed ($\Delta = 0$) the only ratchet effect is the one predicted in Eq. (4), i.e. no inversion is observed.

In order to obtain the first experimental evidence of this newly discovered ratchet effect, we have built a macroscopic realization of our model, i.e. a setup where the thermal bath is replaced by a fluidized granular gas. In such a setup the collisions are unavoidably inelastic: nonetheless, by tuning the collision frequency, it is possible to disentangle the two ratchet mechanisms which act in opposite directions, and so demonstrate the newly discovered effect induced by Coulomb friction. Our setup consists of a rotator vertically suspended in a granular medium (see Fig. 3a) maintained by an electrodynamic shaker in a (roughly homogeneous) stationary gaseous regime [15, 30]. The statistics of the velocities of the grains, on the rotation plane, has been verified to be indistinguishable from a Maxwell-Boltzmann distribution [27]. The shaker performs a vertical sinusoidal oscillation at a frequency of 53 Hz, while the amplitude is varied to explore different regimes of the system. We stress that the rotator is not in direct contact with the shaker, it only collides with the flying grains. Its motion is recorded by an angular encoder which also supports it through two precision spherical bearings. Two rotators have been realized to reproduce the two different shapes of Fig. 1c. The asymmetry of the latter can be inverted

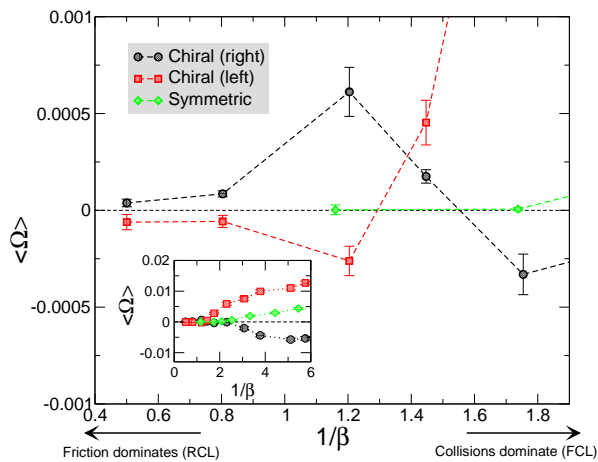


FIG. 4: Real experiment. Plot of the rescaled angular velocity of the rotator, $\langle \Omega \rangle = \frac{R_L}{\epsilon v_0} \langle \omega \rangle$, averaged on an 8-hours run, as a function of β^{-1} which estimates the ratio of time-scales $\frac{\tau_A}{\tau_c}$. The main plot shows the region where a maximum and a current inversion are observed for the asymmetric rotator. The inset sums all the results up, highlighting the behaviour for large β^{-1} . Experiments are performed with maximum shaker acceleration varying in the range from 5 to 20 in gravity units.

(from left to right hand, and vice versa) simply by turning the rotator upside-down. The amplitude of the shaker oscillation is varied to span a range of maximum acceleration (in units of gravity acceleration) between 5 to 20, resulting in a granular thermal velocity v_0 ranging between ~ 100 mm/s and ~ 600 mm/s. Details of the experimental setup and measurement of the parameters are in [27].

In Fig. 3b, we provide some runs demonstrating the ratchet effect for the asymmetric rotator. A net drift is evident when a chiral rotator is used. Turning the rotator upside down results in a reversed direction of rotation. The symmetric rotator makes a diffusive motion with only a small drift revealing the presence of some bias due to imperfections in the rotational symmetry of the setup. Such a bias affects also the curves pertaining to the asymmetric rotator and it does not appear to depend on the rotator's direction of asymmetry, or absence thereof. The typical instantaneous velocity of rotators goes from $\sim 10^{-1}$ to ~ 1 rad/s, much larger than the typical ratchet drift, which goes from $\sim 10^{-4}$ to 10^{-2} rad/s. Such a low signal-to-noise ratio makes it impossible to determine the true behaviour of the rotator if one monitors its position only for short times (e.g. less than a few hours), as evidenced in the inset of Fig. 3b.

In Fig. 4, we show the average adimensional angular velocity $\langle \Omega \rangle = \frac{R_L}{\epsilon v_0} \langle \omega \rangle$ for a set of experiments with asymmetric and symmetric rotators. The behaviour with β^{-1} strongly resembles that observed in our numerical simulations (Fig. 2). At $\beta^{-1} < 1$, we measure $|\langle \Omega \rangle|$ increasing with β^{-1} , followed by a maximum in the proximity of

$\beta^{-1} \sim 1$ and then by an inversion of direction of motion. At large β^{-1} , $|\langle \Omega \rangle|$ increases and finally reaches a plateau (see the inset of Fig. 4). Even with some quantitative discrepancies, we can claim that our experiment reproduces very well the qualitative phenomenology of the model, including the resonant maximum and the inversion point, which are both evidence of the presence of the friction-induced ratchet mechanism. We believe that the quantitative differences (the real ratchet is faster roughly by a factor 2 in the RCL and a factor 5 in the FCL) can be imputed to the many assumptions present in the model, the most important being molecular chaos and spatial homogeneity, hardly controlled in the experiment: indeed non-equilibrium correlations may well become important at high collision frequencies [31].

To conclude, our main discovery is the existence of a minimal ratchet model made of two simple ingredients: a wheel subject to Coulomb friction and a bath at thermodynamic equilibrium. Such a model appears even simpler than the classical Feynmann-Smoluchowsky model [9]. The observation in the laboratory of a maximum and an inversion of the ratchet velocity (Fig. 4), due to the crossover from the inelasticity-dominated (FCL) to the friction-dominated (RCL) regime, is a strong experimental demonstration of the efficiency of this effect. We wish to remark that, in all previous experimental and theoretical work on friction-driven ratchets [32–35], the energy injection was provided by mechanisms different from an equilibrium bath: our proposal is the first which can be realized at the micro- and nano-scale in an equilibrium fluid, that is, without the application of any external field.

We would like to thank A. Vulpiani for useful comments and MD. Deen for technical support. The authors acknowledge the support of the Italian MIUR under the grants: FIRB-IDEAS n. RBID08Z9JE, FIRBs n. RBF081IUK and n. RBF08M3P4, and PRIN n. 2009PYYZM5.

SUPPLEMENTAL MATERIAL

Details of the theory

We recall here some of the main quantities of our model (refer to Figure 1 for a visual explanation of symbols). A rigid body of momentum of inertia I and total mass M is bound to rotate around a fixed axis (say \hat{z}) and is suspended in a molecular or granular fluid. The body is constituted by the set of material points with cartesian coordinates $\{x, y, z\}$ with $z \in [0, h]$ (where h is the height of the cylinder) and $\sqrt{x^2 + y^2} < r(s)$ for each $s \in [0, S]$ where s is the curvilinear abscissa, $r(s)$ is the curve delimiting a section of the solid in the xy plane, and S is the perimeter of the section. The fluid surrounding the rotator has number density n and is made of identical

spheres of mass m . We denote by ω the angular velocity of the rotator, by θ its angular position, and by \mathbf{v} the velocity of a molecule of the fluid. We also denote by $\rho = nh$ the two-dimensional projection of density, which is the only one which matters in our problem. Note that $\rho S \equiv n\Sigma$ if Σ (as in the Letter) is the total scattering cross section of the rotator against the molecules of the bath.

Inelastic collisions The fluid interact with the rotator by means of inelastic collisions, which change the velocity of the rotator from ω (before the interaction) to ω' (after the interaction) and that of the colliding particle from \mathbf{v} to \mathbf{v}' . In the case of hard-core collisions the scattering event follows the rules

$$\omega' = \omega + (1 + \alpha) \frac{(\mathbf{V} - \mathbf{v}) \cdot \hat{n}}{R_I} \frac{g\epsilon^2}{1 + \epsilon^2 g^2}, \quad (6a)$$

$$\mathbf{v}' = \mathbf{v} + (1 + \alpha) \frac{(\mathbf{V} - \mathbf{v}) \cdot \hat{n}}{1 + \epsilon^2 g^2} \hat{n} \quad (6b)$$

where $\alpha \in [0, 1]$ is the restitution coefficient ($\alpha = 1$ corresponds to elastic collisions), $\mathbf{V} = \omega \hat{z} \times \mathbf{r}$ is the linear velocity of the rotator at the point of impact \mathbf{r} , \hat{n} is the unit vector perpendicular to the surface at that point, and finally $g = \frac{\mathbf{r} \cdot \hat{t}}{R_I}$ with $\hat{t} = \hat{z} \times \hat{n}$ which is the unit vector tangent to the surface at the point of impact.

Equations (6) guarantee that total angular momentum $L\hat{z} = m\mathbf{r} \times \mathbf{v} + I\omega\hat{z}$ is conserved, that relative velocity projected on the collision unit vector is reflected and rescaled by the restitution coefficient, $(\mathbf{V}' - \mathbf{v}') \cdot \hat{n} = -\alpha(\mathbf{V} - \mathbf{v}) \cdot \hat{n}$, and finally that the kinetic energy $K = \frac{m}{2}|\mathbf{v}|^2 + \frac{I}{2}\omega^2$ changes as

$$K' - K = -\frac{(1 - \alpha^2)}{2} [(\mathbf{V} - \mathbf{v}) \cdot \hat{n}]^2 \frac{m}{1 + \epsilon^2 g^2}. \quad (7)$$

A few relations in cartesian coordinates may be useful: $\mathbf{V} = (-\omega r_y, \omega r_x)$ and $\hat{t} = (-n_y, n_x)$. It is also useful to realize that $\mathbf{V} \cdot \hat{n} = -\omega R_I g$.

Transition rates for a Gaussian gas The transition rate for the collisional Markov process reads [24]

$$W(\omega'|\omega) = \rho S \int \frac{ds}{S} \int d\mathbf{v} \phi(\mathbf{v}) \Theta[(\mathbf{V} - \mathbf{v}) \cdot \hat{n}] \times \quad (8a)$$

$$|(\mathbf{V} - \mathbf{v}) \cdot \hat{n}| \delta[\omega' - \omega - \Delta\omega(s)], \quad (8b)$$

$$\Delta\omega(s) = (1 + \alpha) \frac{[\mathbf{V}(s) - \mathbf{v}] \cdot \hat{n}}{R_I(s)} \frac{g(s)\epsilon^2}{1 + \epsilon^2 g(s)^2}, \quad (8c)$$

where $\phi(\mathbf{v})$ is the pdf for the gas particle velocities and the Heaviside step function $\Theta[(\mathbf{V} - \mathbf{v}) \cdot \hat{n}]$ enforces the kinematic condition necessary for impact.

Assuming that the velocities of the molecules of the surrounding fluid obey the Maxwell-Boltzmann statistics $\phi(\mathbf{v}) = \frac{1}{2\pi v_0^2} e^{-\frac{v^2}{2v_0^2}}$, one gets an explicit expression for the

transition rates

$$W(\omega'|\omega) = \frac{\rho S R_I^2}{(1 + \alpha)^3 \sqrt{2\pi} \epsilon^2 v_0} \int \frac{ds}{S} |\omega' - \omega| \frac{(1 + \epsilon^2 g^2)^2}{\epsilon^2 g^2} \times \Theta \left[\frac{\omega' - \omega}{g} \right] \exp \left[-\frac{R_I^2}{2\epsilon^2 v_0^2} \left(\omega \epsilon g + \frac{(\omega' - \omega)(1 + \epsilon^2 g^2)}{(1 + \alpha)\epsilon g} \right)^2 \right]. \quad (9)$$

Average velocity in the RCL When $\beta^{-1} \ll 1$ ($\tau_\Delta \ll \tau_c$, denoted as Rare Collisions Limit, RCL), the dynamics is dominated by the rotator at zero velocity with random and independent perturbations due to sparse collisions with gas particles [22]. In this case, the dynamics after each collision event produces an increment of the angular position of the rotator $\Delta\theta$ which depends on the velocity \mathbf{v} of the gas particle, precisely on its projection $v = \mathbf{v} \cdot \hat{n}$, and on the point of impact represented for instance by its curvilinear abscissa s . The formula in the limit of negligible viscous damping ($\gamma_a \rightarrow 0$) is

$$\Delta\theta(v, s) = \sigma(\omega_0) \frac{\omega_0^2}{2\Delta} \quad (10)$$

$$\omega_0 = -(1 + \alpha) \frac{v}{R_I} \frac{\epsilon^2 g}{1 + \epsilon^2 g^2}. \quad (11)$$

As a consequence, the average velocity of the ratchet reads [22]

$$\langle \omega \rangle = \frac{\rho S}{2\Delta} \int dv |v| \phi(v) \Theta(-v) \int \frac{ds}{S} \sigma(g) \frac{v^2}{R_I^2} \frac{(1 + \alpha)^2 \epsilon^4 g^2}{(1 + \epsilon^2 g^2)^2} = \frac{\rho S}{\sqrt{2\pi} \Delta} \frac{\epsilon^4 v_0^3}{R_I^2} \left\langle (1 + \alpha)^2 \sigma(g) \frac{g^2}{(1 + \epsilon^2 g^2)^2} \right\rangle_{surf}. \quad (12)$$

where we have used the shorthand notation for the average along the perimeter of the rotator's shape $\langle \rangle_{surf} = \int \frac{ds}{S}$. If one considers the expression for the control parameter β^{-1} we can finally write for the adimensional angular velocity $\Omega = \frac{R_I \omega}{\epsilon v_0}$

$$\langle \Omega \rangle = \sqrt{\pi} (1 + \alpha)^2 \beta^{-1} \epsilon^2 \left\langle \frac{\sigma(g) g^2}{(1 + \epsilon^2 g^2)^2} \right\rangle_{surf}. \quad (13)$$

Details of the simulations

We have simulated the model described in equations (2) of the Letter, through a suitable adaptation of the Direct Simulation Monte Carlo method (DSMC) [29]. The DSMC is devised to solve numerically a Boltzmann equation, therefore enforcing the Molecular Chaos assumption. In our specific problem, however, the procedure is drastically simplified, since only one particle (the rotator) is represented in the simulation, through its angular velocity and position, ω and θ respectively. The surrounding gas is represented by its constant velocity

distribution $\phi(\mathbf{v})$ (assumed Gaussian with variance v_0^2), unaffected by collisions. The dynamics of these variables advances by a series of constant and small time steps of length δt taken smaller than all characteristic time-scales in the problem. At every time step a *free streaming* update and a *collisional* update are performed. The free streaming corresponds to the evolution of ω and θ from t to $t + \delta t$ in the absence of any interrupting collisions. In the *collisional* update, a collision is performed with the probability dictated by the Boltzmann equation (Eq. (3) of the Letter). The correct probability is sampled through a Monte Carlo procedure, where a *tentative* collision is proposed, by choosing the point of impact (at random and uniformly) along the surface of the rotator and by extracting the velocity \mathbf{v} with probability $\phi(\mathbf{v})$. The *tentative* collision is realized with a probability equal to $p_c = (\mathbf{V} - \mathbf{v}) \cdot \hat{n} \rho S \delta t$ (note that δt is chosen much smaller than τ_c and this guarantees that $p_c \ll 1$), leading to an update of ω by the collision rule. Otherwise no collisions occur. Note that the choice of the point of impact (which determines also \hat{n}) can reproduce the precise shape of the experimental rotator (symmetric or chiral).

Control parameter β^{-1} as a good estimate of the ratio of typical times. In Figure 5 we report the ratio between the collision times τ_c and frictional stop times τ_Δ , observed in the simulations in different regimes, in order to assess the fairness of estimate $\beta^{-1} \approx \tau_\Delta/\tau_c$.

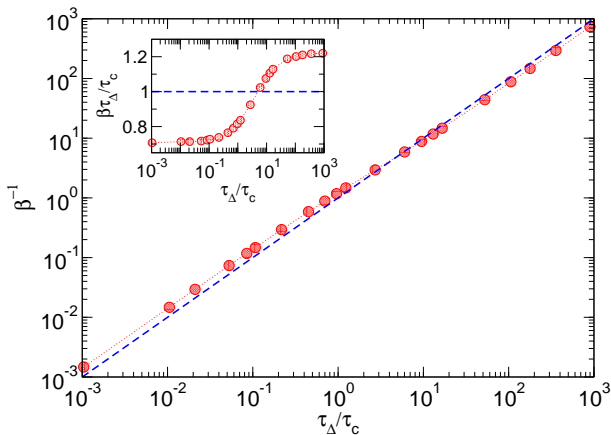


FIG. 5: Assessment of the estimate β^{-1} for τ_Δ/τ_c . The ratio between τ_Δ/τ_c and β^{-1} obtained in numerical simulations is shown in the inset. The estimate is useful in experiments, where measurements of τ_Δ and τ_c are not reliable. It is seen that the estimate is a good approximation of the time-scale ratio where it is close to 1, while it slightly deviates from it in the RCL and FCL, by a factor ~ 1.25 and ~ 0.7 respectively.

Experimental set-up.

We assume that the evolution of the angular velocity ω of the rotator obeys an equation of the form

$$I\dot{\omega}(t) = -F_{friction}\sigma[\omega(t)] - \Gamma_{visc}\omega(t) + F_{coll}(t), \quad (14)$$

where I is the momentum of inertia, $F_{friction}$ is the dry friction torque, σ the sign function and Γ_{visc} the air viscous drag. The term $F_{coll} = I\eta_{coll}$ contains the driving torque, that is the angular momentum randomly transferred from the beads to the rotator, and is analysed in detail in Section 2. We refer to Figure 3a of the paper for the main features of our set-up. Dissipation coefficients rescaled by inertia are $\gamma_a = \Gamma_{visc}/I$ and $\Delta = F_{friction}/I$.

Technical details about the experimental setup. The granular medium, made of 50 polyoxymethylene (POM) spheres (radius $r = 3$ mm and mass $m = 0.15$ g), is housed in a polymethyl-methacrylate (PMMA) cylinder (diameter 90 mm) with a conical-shaped floor. A removable cap encloses a miniaturized angular encoder (model AEDA-3300 by Avago Technologies). The encoder, which also supports the rotator, provides high resolution measurements (up to 80,000 division/revolution at the maximum rate of 20 kHz) of the rotator position. The system is vibrated by an electrodynamic shaker (model V450 by LDS Test & Measurement) fed by a sinusoidal excitation. An accelerometer measures the actual acceleration induced to the system. A high-speed camera (EoSens CL by Mikrotron) tracks single beads in order to measure their velocity. The two rotators are made of PMMA, have height $h = 15$ mm and are distinguished by their different section on the rotation plane. The momentum of inertia of the rotator I comprises different parts. The probe is attached to the angular encoder by means of a steel rotation axis 50 mm high and 3 mm thick. The mass of the whole rotator (axis and probe) is $M = 5.21$ g for the asymmetric probe and $M = 6.49$ g for the symmetric one. The total momentum of inertia is $I = 135$ gmm² and $I = 353$ gmm² for the two types, respectively. In both cases the inertia of the axis is a few hundredths of the total one. The shape factors of the asymmetric rotator, relevant for its ratchet effect, are $\left\langle \frac{\sigma(g)g^2}{(1+\epsilon^2g^2)} \right\rangle_{surf} = 0.0013$ and $\frac{\langle g^3 \rangle_{surf}}{\langle g^2 \rangle_{surf}} = 0.052$ for the RCL and FCL limits respectively (see text for definitions). Both the shape factors vanish for the symmetric rotator.

Dry and viscous friction. The only source of dry friction comes from the two ball bearings inside the encoder while viscous friction is due to the air surrounding the rotator. We measure the dry and viscous friction during a standard experimental run (eight hours), but considering only periods where the rotator is subject to these forces and no other: $\dot{\omega} = -\gamma_a\omega \mp \Delta$ (where the upper sign holds for $\omega > 0$ and the lower for $\omega < 0$), i.e. excluding the time immediately about collisions and periods of rest. Angular

velocity and acceleration are obtained from the angular position (in function of time) by differentiation. A bidimensional histogram is calculated and a peak-finding procedure has been applied in order to obtain the most probable trajectories in $(\omega, \dot{\omega})$ space. Finally, the most probable trajectory is fitted with the above linear equations, yielding the values $F_{friction} = (9.9 \pm 0.7) \times 10^3 \text{ g mm}^2/\text{s}^2$ and $\Gamma_{visc} = (1.6 \pm 0.2) \times 10^3 \text{ g mm}^2/\text{s}$. It is interesting to notice that viscous friction becomes important for velocities larger than the threshold velocity $\omega_{th} = F_{friction}/\Gamma_{visc} \approx 6.2 \text{ s}^{-1}$, separating the friction-dominated regime $\omega \ll \omega_{th}$ from the viscosity-dominated one $\omega \gg \omega_{th}$.

Restitution coefficients. The beads-rotator restitution coefficient α has been measured launching a single bead against the rotator while recording the rotator position at high sampling rate (1 kHz). For these measurements the top of the apparatus is removed and put with the rotation axis parallel to the floor. A bead falls from height h and hits the rotator with velocity $v = \sqrt{2a_g h}$ (here a_g indicates the gravity acceleration). The high-speed camera has been used to monitor the exact distance x of the impact point from the rotation axis. We calculate the restitution coefficient using the collision rule (see Section 2 below) adapted for this particular configuration in which the rotator is at rest before the collision ($\Omega = V = 0$) and $g \approx x/R_I$. In this circumstances the velocity of the rotator after a collision is $\omega' = (1 + \alpha)vx/(I/m + x^2)$. Repeated measurements on the symmetric rotator gave the following results: $\alpha = 0.83 \pm 0.16$ (we recall that $\alpha = 1$ for elastic collisions).

Granular gas velocity statistics. We discuss here the methods used to characterize the velocity statistics of the granular gas. A fast camera (EoSens CL by Mikrotron) is placed above the PMMA container to catch horizontal components of motion (v_x, v_y) of the polyoxymethylene (POM) spheres constituting the granular gas. Focus of lens is adjusted to the plane at half height of the probe. Lighting is provided by a led-dome which diffuses light on the system reducing shadows and reflections. Particle tracking is enhanced by marking a few tracers: 3 POM spheres are white, while all the other particles are black. Pictures are taken at 250 frames per second: this is verified to be the optimal compromise between too large delays, which prevent tracking of ballistic trajectories, and too small ones, which produce “false movement” induced by noise due to finite sensitivity of the camera resolution and the centring algorithm. Uncertainty in the determination of the centre of mass of tracer spheres is estimated to be $\sim 0.05 \text{ mm}$. The details of velocity measurements and error estimates are reported in [36]. In Figure 6 we display a typical snapshot of the system from the camera (see also the accompanying Movie).

For each choice of shaking parameters we have computed the velocity histogram from a series of 2×10^4 contiguous frames. Examples of those histograms are re-

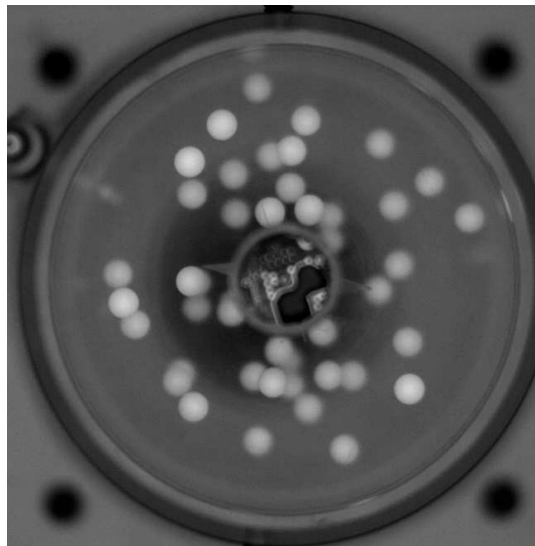


FIG. 6: A snapshot of the system taken from the fast camera (shaker is vibrating at 53 Hz with rescaled maximum acceleration $\Gamma = 8$).

ported in Figure 7, left frame. A Gaussian fit is seen to be a good approximation and provides the value of $v_0 = \sqrt{\langle v^2 \rangle}$ where v is v_x or v_y (isotropy is always verified). In the right frame of Figure 7 we report the values of v_0 as function of the rescaled maximum acceleration $\Gamma = \frac{a_{max}}{a_g}$ where a_g is gravity acceleration and the $z_s(t)$ position of the shaker’s vibrating head follows the law $z_s(t) = \frac{a_{max}}{(2\pi f)^2} \sin(2\pi f t)$ with f being the vibration frequency.

Rotator velocity signal. An example of the velocity signal $\omega(t)$ in two different regimes (frequent and rare collisions) is shown in Figure 8, left frame, for the case of the symmetric rotator. In the right frame of the same Figure, we show the angular velocity autocorrelation $C(t) = \langle \omega(t)\omega(0) \rangle - \langle \omega \rangle^2$ versus time. Note that the signal average is much smaller than its standard deviations and, hence, it is negligible in $C(t)$.

Here, it is interesting to comment about the smaller characteristic time associated to the system with rare collisions (red curve), with respect to that with frequent collisions (black curve): this is a consequence of the smaller typical velocity in the rare collisions configuration, which induces faster relaxations through Coulomb friction dissipation (we recall that $\tau_\Delta \approx \frac{\langle \omega \rangle}{\Delta}$). Similar results are obtained with the asymmetric rotator.

-
- [1] T. L. Hill, *Thermodynamics of Small Systems* (Dover Publications, New York, 1964).
 - [2] M. Schliwa and G. Woehlke, *Nature* **422**, 759 (2003).
 - [3] S. Rice *et al.*, *Nature* **402**, 778 (1998).
 - [4] I. Rayment *et al.*, *Science* **261**, 50 (1993).

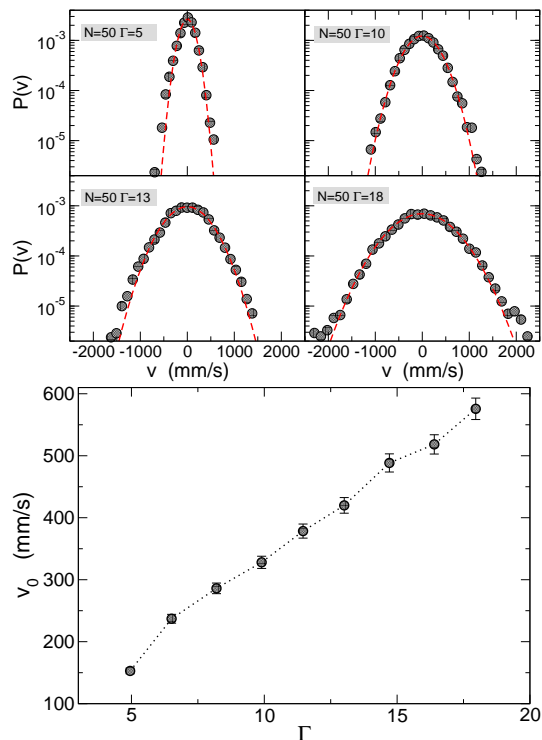


FIG. 7: Left: Histograms of velocities (v_x) of $N = 50$ granular gas particles for different values of the rescaled maximum acceleration Γ at vibration frequency 53 Hz. Gaussian fits are superimposed. Right: the values of v_0 (standard deviation) versus Γ .

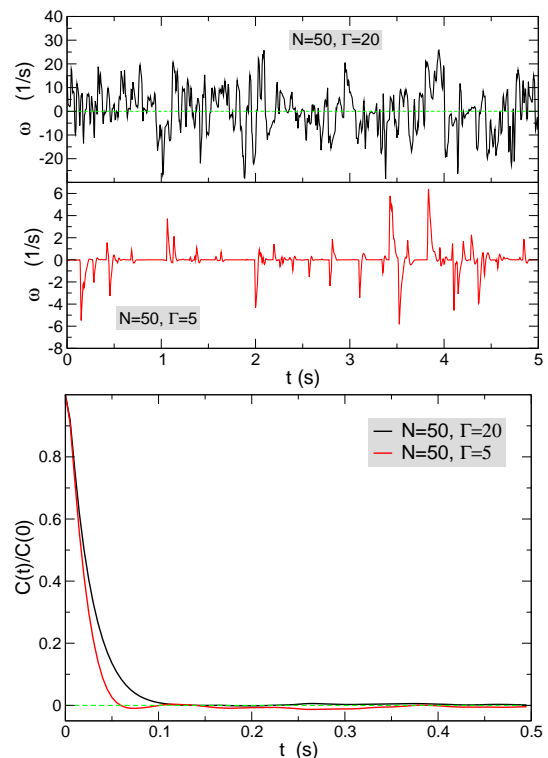


FIG. 8: Left: Examples of symmetrical rotator's angular velocity signal $\omega(t)$ as acquired from the angular encoder at 200 Hz in two different regimes (frequent collisions, top, and rare collisions, bottom). Right: rescaled angular velocity autocorrelation $C(t)/C(0)$ versus time t for the two cases shown in the left frame.

- [5] R. Di Leonardo *et al.*, Proc. Natl. Acad. Sci. USA **107**, 9541 (2010).
- [6] A. Sokolova, M. M. Apodacac, B. A. Grzybowski and I. S. Aranson, Proc. Natl. Acad. Sci. USA **107**, 969 (2010).
- [7] G. Gradenigo, A. Sarracino, D. Villamaina, T. Grigera and A. Puglisi, J. Stat. Mech. L12002 (2010).
- [8] M. v. Smoluchowski M v, Phys. Z. **13**, 1069 (1912).
- [9] R. P. Feynman, R. B. Leighton and M. Sands M, *The Feynman Lectures on Physics* (Addison-Wesley, Reading, MA, 1963), Vol. I, Cap. 46.
- [10] M. M. Magnasco, Phys. Rev. Lett. **71**, 1477 (1993).
- [11] R. D. Astumian, Science **276**, 917 (1997).
- [12] P. Reimann, Phys.Rep. **361**, 57 (2002) .
- [13] P. Hänggi and F. Marchesoni, Rev. Mod. Phys. **81**, 387 (2003).
- [14] H. M. Jaeger, S. R. Nagel, R. P. Behringer, Rev. Mod. Phys. **68**, 1259 (1996).
- [15] G. D'Anna *et al.*, Nature **424**, 909 (2003).
- [16] Z. Farkas, P. Tegzes, A. Vukics and T. Vicsek, Phys. Rev. E **60**, 7022 (1999).
- [17] P. Eshuis, K. van der Weele, D. Lohse and D. van der Meer, Phys. Rev. Lett. **104**, 248001 (2010).
- [18] R. Balzan, F. Dalton, V. Loreto, A. Petri and G. Pontuale, Phys. Rev. E **83**, 031310 (2011).
- [19] G. Costantini, A. Puglisi and U. Marini Bettolo Marconi, Phys. Rev. E **75**, 061124 (2007).
- [20] B. Cleuren B and C. Van den Broeck, Europhys. Lett. **77**, 50003 (2007).
- [21] G. Costantini, U. Marini Bettolo Marconi and A. Puglisi, Europhys. Lett. **82**, 50008 (2008).
- [22] J. Talbot, R. D. Wildman and P. Viot, Phys. Rev. Lett. **107**, 138001 (2011).
- [23] J. Talbot, A. Burdeau and P. Viot, J. Stat. Mech. P03009 (2011).
- [24] B. Cleuren and R. Eichhorn, J. Stat. Mech. P10011 (2008).
- [25] B. N. J. Persson, *Sliding Friction* (Springer, Berlin, 1998).
- [26] R. Guerra, U. Tartaglino, A. Vanossi and E. Tosatti, Nature Materials **9**, 634 (2010).
- [27] See Supplemental Material at [URL will be inserted by publisher] for details on experimental setup, theory and simulations.
- [28] N. G. van Kampen, Can. J. Phys. **39**, 551 (1961).
- [29] G. A. Bird, *Molecular Gas Dynamics and the Direct Simulation of Gas Flows* (Clarendon, Oxford, 1994).
- [30] A. Naert, Europhys. Lett. **97**, 20010 (2012).
- [31] G. Gradenigo, A. Sarracino, D. Villamaina and A. Puglisi, Europhys. Lett. **96**, 14004 (2011) and A. Sarracino, D. Villamaina, G. Gradenigo, A. Puglisi, Europhys. Lett. **92**, 34001 (2010).
- [32] M. Eglin, M. A. Eriksson and R. W. Carpick, Appl. Phys. Lett. **88**, 091913 (2006).
- [33] A. Buguin, F. Brochard and P.-G. de Gennes, Eur. Phys. J. E **19**, 31 (2006).
- [34] D. Fleishman, J. Klafter, M. Porto and M. Urbakh, Nano Lett. **7**, 837 (2007).

- [35] A. Baule and P. Sollich, *Europhys. Lett.* **97**, 20001 (2012).
- [36] A. Puglisi, A. Gnoli, G. Gradenigo, A. Sarracino and D.

Villamaina, *J. Chem. Phys.* **136**, 014704 (2012).